# THE EFFECTS OF POLOXAMER 188 ON WOUND CLOSURE IN A MOUSE BRAIN ENDOTHELIUM MODEL

By

Mia Claire Grubbs

Presented to the Faculty of the Graduate School of
The University of Texas at Arlington
Submitted in Partial Fulfillment of the Requirements for the Degree of

Master of Science in Biomedical Engineering

Supervising Professor:
Michael Cho, Ph.D. FAIMBE
Professor and Chair of Bioengineering Department
The Alfred R. and Janet H. Potvin Endowed Chair

THE UNIVERSITY OF TEXAS AT ARLINGTON
December 2023

# Acknowledgments

Thank you to Dr. Michael Cho, my supervising professor, for choosing to give me the opportunity that would change the trajectory of my educational journey. Thank you for your guidance, support, and the chance to further develop research that will one day change lives.

Thank you to Dr. Nagham Alatrash for holding my hand in the early days and continuing to walk me through the steps to build a strong foundation for my continuing wet lab research.

Thank you to my peers turned best friends, Anne and Kelli for the ongoing support in and outside of the lab.

And I express my gratitude to Drs. Alfred R. and Janet H. Potvin for the financial support that made this research possible.

# Abstract

The blood-brain barrier (BBB) plays a crucial role in maintaining central nervous system homeostasis and, if structurally and functionally compromised, can lead to severe neurological consequences. This thesis explores the therapeutic potential of Poloxamer 188 (P188) in the context of BBB wound healing. P188, FDA-approved copolymer that is known for its cytoprotective properties, is examined for its impact on endothelial monolayers through in vitro scratch wound assays. The study aims to establish a consistent endothelial monolayer model, quantify wound healing dynamics, and assess the efficacy of P188 at varying concentrations. The thesis goals include detailed methodologies such as cell culture techniques, scratch wound modeling, and treatment with P188. Results indicate that P188 significantly influences the rate of wound closure, with concentrations as low as 10 uM, and using a higher concentration (e.g., 100 uM) did not further accelerate wound healing. An automated wound detection algorithm was developed to quantify the characteristics of wound closure. While this algorithm was sufficient to analyze the initial wound size and morphology, ImageJ FIJI software had to be employed for manual wound area analysis at later stages. Our findings suggest the need for further exploration of more complex wound morphology and an in-depth understanding of the wound healing mechanisms that are mediated by P188. Future work may involve investigating P188's impact on cell proliferation and migration. Overall, this research sheds light on the potential of P188 as a therapeutic agent for BBB wound healing, paving the way for future investigations and applications for reparative tissue healing in the brain.

Table of Contents

Table of Figures

# Chapter 1: Introduction

## 1.1 The Blood Brain Barrier (BBB)

The blood-brain barrier (BBB) is a pivotal physiological structure crucial for maintaining central nervous system (CNS) homeostasis [1]. Comprising specialized endothelial cells, tight junctions, and supporting cells, the BBB acts as a formidable defense mechanism, regulating substance passage between the bloodstream and the brain [2]. Its primary functions include preserving the microenvironment of the brain and orchestrating a selective filtration system that permits essential nutrients while preventing harmful substances from reaching the neural tissue (Fig. 1). This selective permeability is vital for maintaining the delicate balance necessary for neural signaling, synaptic transmission, and overall CNS function [3]. However, when the BBB integrity is compromised due to injury, inflammation, or underlying diseases, it can have serious consequences [4]. A breakdown in BBB integrity leads to increased permeability, allowing potentially harmful substances to enter the brain parenchyma [5]. This breach can result in neuroinflammation, oxidative stress, and neuronal damage, contributing to the pathogenesis of various neurological disorders [6]. Additionally, a compromised BBB facilitates the entry of immune cells, increasing inflammatory responses within the CNS [7].

ZO-1 is a protein that plays a crucial role in the formation and maintenance of tight junctions in endothelial cells. Tight junctions are specialized intercellular junctions that form a barrier between adjacent cells, regulating the passage of ions, water, and various molecules. ZO-1 interacts with other tight junction proteins and the actin cytoskeleton, helping to anchor the tight junction complex to the cell's cytoskeleton and stabilizing the junctional complex [8].

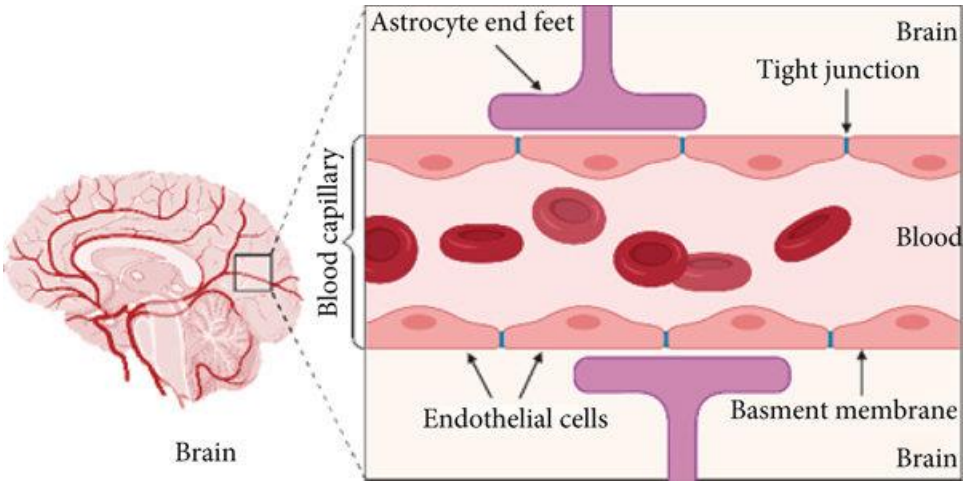


***Figure 1****: Schematic of the Blood Brain Barrier illustrating important features [9] such as intact endothelium that is often visualized by tight junction molecules (e.g., ZO-1 proteins).*

## 1.2 Modeling an Endothelial Wound In Vitro

The in vitro modeling of wound healing in monolayers of endothelial cells has been a subject of significant research [10][11], contributing to the understanding of cellular responses and repair mechanisms. These studies often involve controlled disruptions to the endothelial cell monolayer, providing insights into wound closure dynamics and the factors influencing recovery. Prior research has successfully utilized in vitro wound models to investigate the regenerative capacity of endothelial cells within monolayers. These models often employ techniques such as scratch assays or mechanical injury to simulate wounds, allowing for observation and quantification of cell migration, proliferation, and the re-establishment of cell-cell junctions [12]. The scratch assay, for example, involves creating a controlled wound in the monolayer and subsequent monitoring of cell migration to fill the gap, providing valuable information on the healing process [13][14][15]. These studies on endothelial cell monolayers have contributed to unraveling the molecular and cellular events associated with wound repair. Key signaling pathways have been identified, including growth factors and adhesion molecules involved in the

migration and proliferation of endothelial cells during the healing process [16]. By extending the principles of wound modeling to the context of the blood-brain barrier, injury to the endothelial cell monolayer can closely mimic the conditions of the BBB. Understanding the response of endothelial cell monolayers to wounds leads to further exploration into the effects of injury, inflammation, and oxidative stress on the BBB.

### 1.3 Investigating Poloxamer 188 (P188)

Poloxamer 188 (P188), a nonionic block copolymer surfactant, has emerged as a promising candidate in various therapeutic applications since its discovery in the 1950s. Initially recognized for its efficacy in preventing blood cell damage during cardiac bypass surgery, P188's unique properties have caught the attention of researchers for its potential in diverse medical conditions, particularly wound healing. Prior studies have indicated that P188 demonstrates cytoprotective properties in a range of applications such as burns, ischemia, and trauma [17][18][19]. Its capacity to decrease inflammation, function as an antithrombotic and anti-sludging agent, and enhance microvascular blood flow highlights how versatile it is in managing the complex processes of wound healing. Further, the ability of P188 to bind to exposed hydrophobic domains is known to be crucial in restoring non-adhesive surfaces and preventing the activation of harmful inflammatory, coagulation, and apoptotic reactions. However, the precise mechanisms of the poloxamer are still under investigation [20][21].

# Chapter 2: Hypothesis

The overall hypothesis of the reparative effects of P188 to close the wound at an accelerated pace will be validated or refuted by the two specific aims. Evaluation of the effects of P188 will be conducted by two existing imaging analysis methods and explore the potential for a new computer-automated analysis of detection of the wound edge.

## Aim 1.

The primary objective of this thesis is to lay the foundational groundwork for investigating the therapeutic potential of Poloxamer 188 (P188) in the context of wound healing in the BBB. The wound model will be used to determine consistency and reproducibility when exploring the effects of different P188 concentrations on the healing rate of the endothelial monolayer. The goal is to identify a range of P188 concentrations that facilitate therapeutic benefits, such as enhanced wound closure, reduced inflammation, and improved cellular responses.

## Aim 2.

Building on the establishment of a consistent endothelial monolayer in Aim 1, the second objective of this thesis is to explore the intricate process of quantifying and analyzing wound healing dynamics over time. By utilizing ImageJ FIJI for high-resolution manual analysis of wound closure, the rate of closure and suitable treatment concentration will be determined. Additionally, the aim explores the feasibility of a computer-automated wound edge detection method to quantify wound closure.

# Chapter 3: Methods and Materials

## 3.1 Cell Culture

BALB/c Mouse Primary Brain Microvascular Endothelial Cells (MPBMEC's, Cat. No. BALB-5023) were sourced from Cell Biologics and cultured in a complete medium, Endothelial Cell Medium (ECM, Cat. No. C57-1001) supplemented with 5% fetal bovine serum (FBS, Cat. No. FBS-5001) and 1% endothelial cell growth supplement (ECGS, Cat. No. C57-1003) at 37°C with 5% CO2. To promote cell adhesion, culture dishes were pre-coated with Gelatin-Based Coating Solution (Cat. No. C57-1021). Subculturing involved treating BEC's with 0.25% Trypsin-EDTA solution (Cat. No. 6914), neutralizing trypsin with complete medium, and centrifuging cells at 1000 RPM for 5 minutes. The resuspended cells were then plated in gelatin-coated dishes, with regular microscopic monitoring and medium changes every 24-48 hours. For assessing cell confluency and viability, a hemocytometer was employed. Cells, mixed with 0.4% Trypan Blue, underwent counting in both corner and center grids for representative sampling. The cell concentration (cells/mL) was calculated using the formula: Cell concentration = (Total counted cells ÷ Number of counted squares) × Dilution factor, maintaining a consistent cell concentration of $5 \times 10^5$ cells/mL for all experimental conditions.

## 3.2 Wound Model

To create the wound model, the BEC's were plated onto 15 mm glass bottom culture dishes (CellTreat Tissue Culture Dish 229632), 300 uL of suspended cells were seeded onto each plate and after 4 days of growth or full confluency was reached, the scratches were made. Before creating the scratch wound, the media was removed, and then a sterile 1-10 uL pipette tip was used to create a linear, '+'-shaped injury across the monolayer (Fig. 2). The pipette tip measured 0.8 mm in diameter and created wounds of ~500 um width on average. The tip was carefully

maneuvered to ensure consistent depth and width of the scratch while avoiding unintended disruption of neighboring cells. Complete media or P188 solution was carefully and immediately added back to the dish after wounding to ensure the cell's viability, followed by imaging then returning to incubation until the next imaging period. Media was changed every 12 hours in control plates.

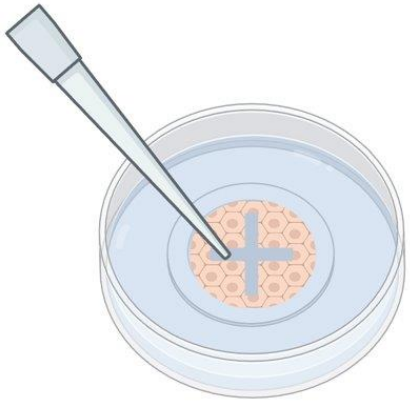

***Figure 2****: Schematic of scratch wound model method demonstrating the use of the "+" shape, made with a 1-10 uL pipette tip, in the monolayer of cells, to better track the region during closure. Schematic made with Biorender [22].*

3.3 Treatment with P188

The Poloxamer 188 purchased from Sigma Aldrich (Kolliphor® P 188) comes in a powder form with a molecular weight of ~7680-9510 g/mol. To make a stock solution of 2 mL concentration of 2 mM, an appropriate amount of P188 powder was emulsified in 2 mL complete endothelial cell media. The stock was further diluted into 100 uM and 10 uM for treatment experiments. For the application of both concentrations of P188 solution, 250 uL was applied to each imaging plate and replaced with full media after 12 hours.

### 3.4 Immunofluorescent Microscopy

To confirm that the BEC's were capable of forming a consistent monolayer prior to damage, ZO-1 immunostaining was used. ZO-1 is a protein crucial for tight junctions and barrier function, so by fluorescently labeling this protein, we can confirm the cell's ability to form a functional monolayer. Cells were first washed gently with PBS to remove the culture medium and then fixed with 4% paraformaldehyde for 10 minutes at room temperature (for PFA fixation). After fixation, cells were rinsed with PBS to remove any remaining fixative. Cells were then permeabilized with 0.1% Triton for 15 minutes and rinsed again with PBS. To block nonspecific binding, cells were incubated in a blocking buffer, 2% BSA for an hour at room temperature. The ZO-1 primary antibody was then diluted with 0.1% BSA, for 4 imaging plates 10 uL ZO-1 plus 990 uL 0.1% BSA allowed 250 uL solution per plate, then applied to the cells, which were incubated for another 1-2 hours at room temperature and kept in the dark.

To track the growth during the scratch experiments, the cells were stained with NucBlue Live ReadyProbes Reagent (Invitrogen, Thermo Fisher Scientific) that binds to DNA and therefore each cell's nucleus was identified and visualized.

One drop of the stain was applied to each imaging dish, incubated for 10-15 minutes, then rinsed 3 times with PBS to remove excess stain then imaged on the same microscope using a DAPI filter. The damage was applied to the cell dishes after staining.

### 3.5 Image Analysis

#### 3.5.1 Hand Drawn ROIs using ImageJ FIJI

Regions of Interest (ROI)'s were manually identified and outlined using the hand-draw tool and ROI manager provided in ImageJ to quantify the wound area over a series of images

(Fig. 3). ImageJ was able to convert the pixel values and quantify the wound area in microns ($um^2$).

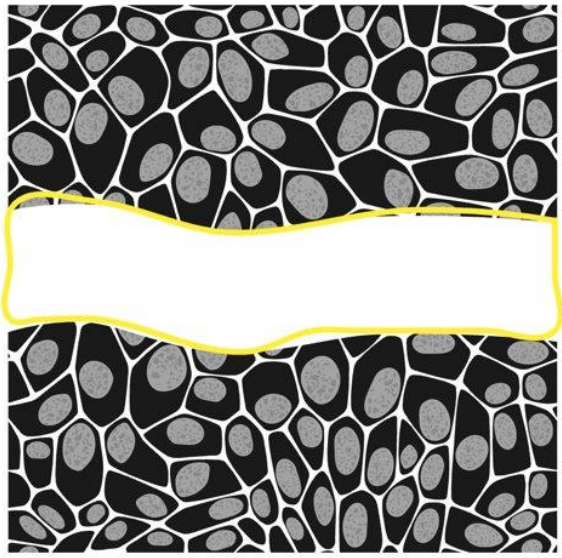

***Figure 3****: Representation of Hand-Drawn region of interest (ROI) at Time = 0 in ImageJ. Made with Biorender [22]. Manual analysis was used because the initial computer-automated method was determined successful only at the initial stages of wound closure (see below for full explanation).*

### 3.5.2 Analyze Particles Cell Counter in ImageJ FIJI

Another feature in ImageJ is the "analyze particle" function that with the addition of a threshold and defined parameters, the software is able the count the number of cells located in the ROI. The hand-drawn ROI from Time = 0 was first assessed for the number of cells, and subsequent measurements were performed at different times to determine the number of cells populating the once vacant area.

### 3.5.3 First Generation Computer Automated Wound Edge Analysis

While the above manual methods are most common in monolayer edge tracking, the need to reduce human error remains high and with the development of software capable of machine

learning, there are new pathways to explore that could more accurately predict the rate of closure in wound models. A basic code was developed in MATLAB that is able to quantify the average intensity of each row of pixels in an image, and then graph the results with fluorescent intensity peaks and valleys that correspond to the wound edges and space between (Fig. 4). This method proved acceptable and consistent for images taken at Time = 0. However, as wound healing progressed, the wound edge became less defined and the wound edge detection algorithm was inadequate and insufficient (see Fig. 4 below). The attempt to automate the method of analysis shows potential for accurately determining the wound edge and even predicting wound closure patterns. The scope of this project's timeline did not allow for completion, however. Until the automated method is further developed and validated, the experiment results generated for this thesis were analyzed by manual methods.

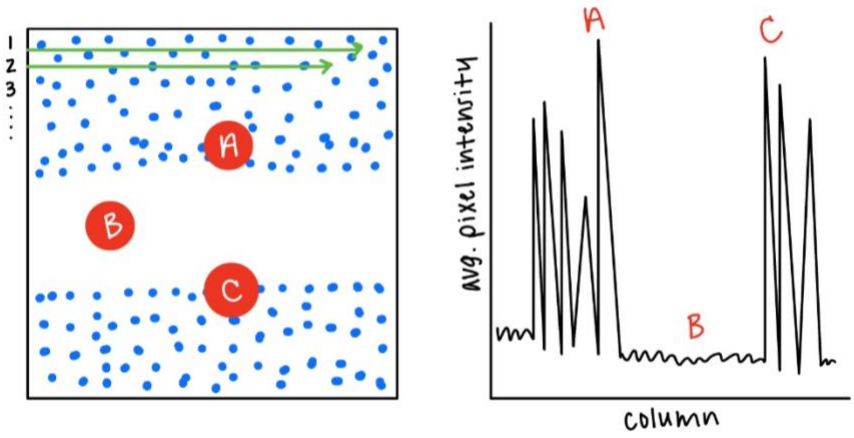


***Figure 4****: Representation of computer-automated wound edge analysis. The green arrows indicate the intensity of pixels in the rows identified and then averaged. Points A and C represent areas of high average pixel intensity indicating a high cell population. Point B indicates low pixel intensity, or where cells are not present, indicating wound area. These areas of high pixel intensity (A & C) represent the peaks in the graph, while the lowest pixel intensity is the valley (B), identifying the scratch.*

# Chapter 4: Results

## 4.1 Establishment of a Monolayer

The initial experiments aimed to achieve the first objective of establishing a functional monolayer with a consistent cell density, setting the groundwork for subsequent wound model experiments. Utilizing a manual hemocytometer and Hemocytometer Sidekick App ensured the maintenance of a consistent seeding cell density of 5 x $10^5$ cells/mL. This standardized cell density served as a crucial baseline for all experiments, ensuring objective assessment of growth rates and providing a consistent starting point for both control and treated samples. Verification of a functional monolayer formation was confirmed through NucBlue and ZO-1 immunostaining, enabling clear identification of nuclei and tight junctions within the cell membranes (Fig. 5).

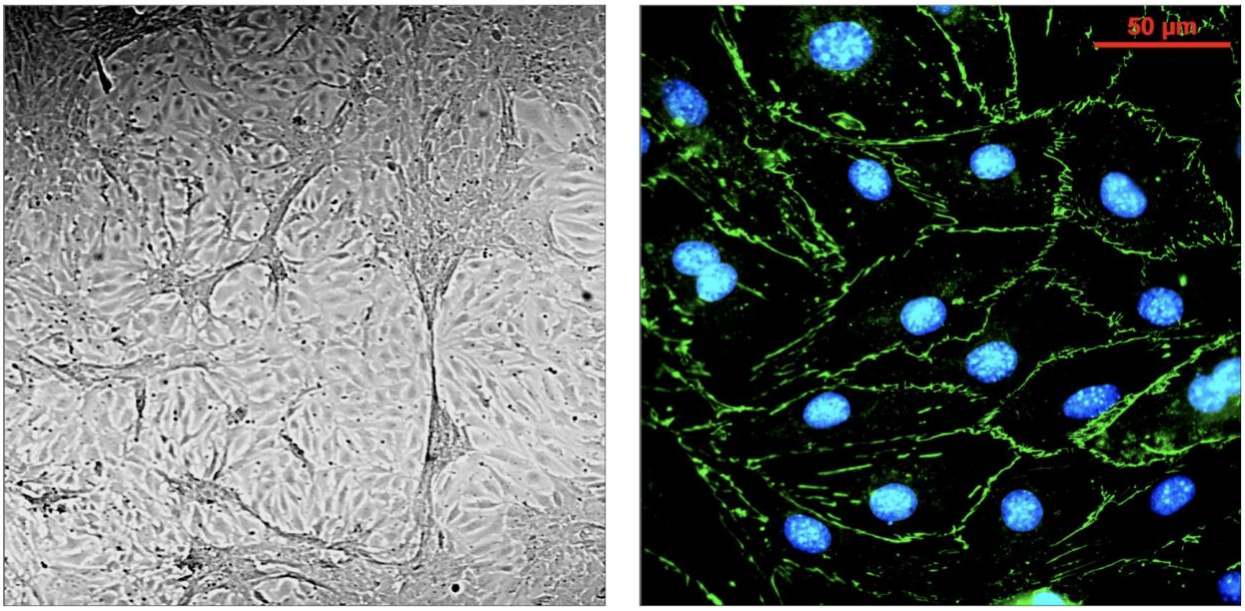


***Figure 5****: A: Bright Field image of brain endothelial cells acquired using a 10x microscope objective after four days of cell culture. B: Immunofluorescent image acquired using a 60x microscope objective of Nucblue stained nuclei (blue) and ZO-1 stained tight junctions (green) after four days of cell culture. This image is deemed necessary to demonstrate the in vitro monolayer model is adequate for the experiments in this thesis.*

### 4.2 Initial P188 Treatments – Replication of a Previous Experiment

Previous investigations on P188's wound healing capabilities typically used higher concentrations. For example, in a mechanically induced wound model, 500 uM P188 was used to repair tissue damage [23]. The first aim of this study therefore sought to replicate the scratch model using treatment concentrations of < 500 uM P188. As indicated in Figure 6, the wound could be identified in the region of no cells in the middle (first column). The cells were visualized with Nucblue which binds to DNA and therefore each nucleus can be identified. Within 18 hours following the initial P188 treatment, the wound closing is qualitatively evident.

### 4.3 Decrease in Treatment Concentration

Subsequent to consistent wound closure outcomes with 100 uM P188, the concentration was further reduced to 10 uM, providing a basis for comparison against the previous 100 uM treatments and a negative control (Fig. 6).

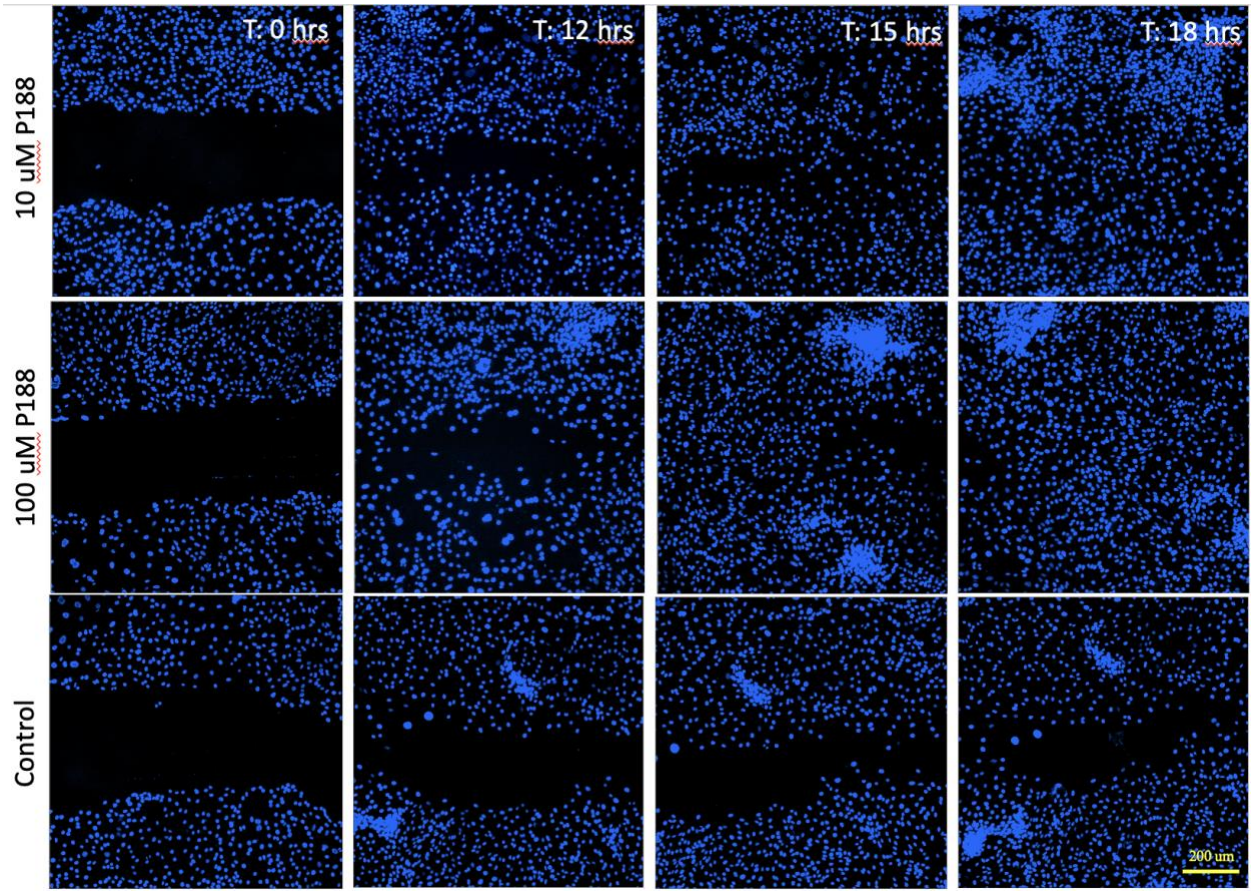


***Figure 6****: Series of images comparing the visual closure of the wound in 10 uM, 100 uM, and control plates captured at time 0, 12, 15, and 18 hours. The 10uM and 100uM images appear to have similar wound closure rates while the control still has nonpopulated area at Time = 18 hours. Visual inspection shows that the P188 treated cells appear to have closed the wound at hour 18 while the not-treated cells still have a noticeable wound size. Bar = 200 um.*

## 4.4 Introduction of Hand-Drawn ROIs

The assessment of the scratch wound area involved ImageJ FIJI software, where the wound's edge was manually outlined and captured in microns. Wound closure efficiency was expressed as a percentage of the average wound area per time point normalized by the initial wound area.

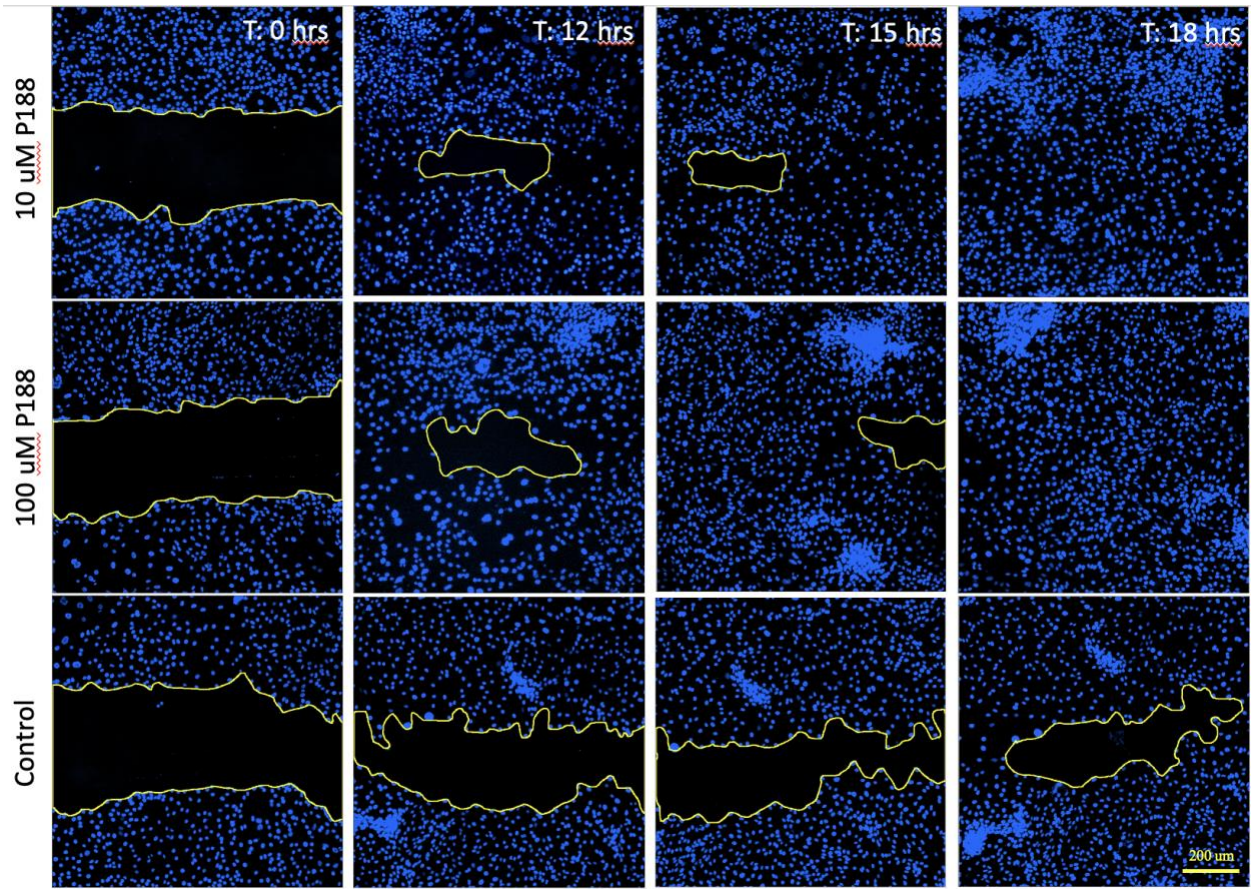


***Figure 7****: Using the images from Figure 6, hand-drawn wound edges utilizing ImageJ are outlined in yellow. It appears manual identification of the wound edge at earlier time points is likely more accurate because the wound is well-defined but not as accurate at later times. Bar = 200 um.*

In order to quantify the wound closing rate, the wound size at different time points from one given set of experiments was determined using ImageJ and normalized by the initial wound size. The same experiment was repeated 3 times using 0, 10, and 100 uM P188. The rate of closure for each instance was calculated by finding the difference between the normalized average value at each time point and then taking the average of that to find the rate over the period as a whole. The rates are as follows [percent wound closure/hour]: 5.28 %/hr (10 uM P188), 5.15 %/hr (100 µM P188), and 3.38 %/hr (control with no P188 treatment). When determining the percent wound closure over time, the wound is assumed to be closing at a

consistent rate throughout the experiment, however this assumption is still being explored. This consistent rate of closure was assessed by fitting a linear line through the data points (see Fig. 8 below).

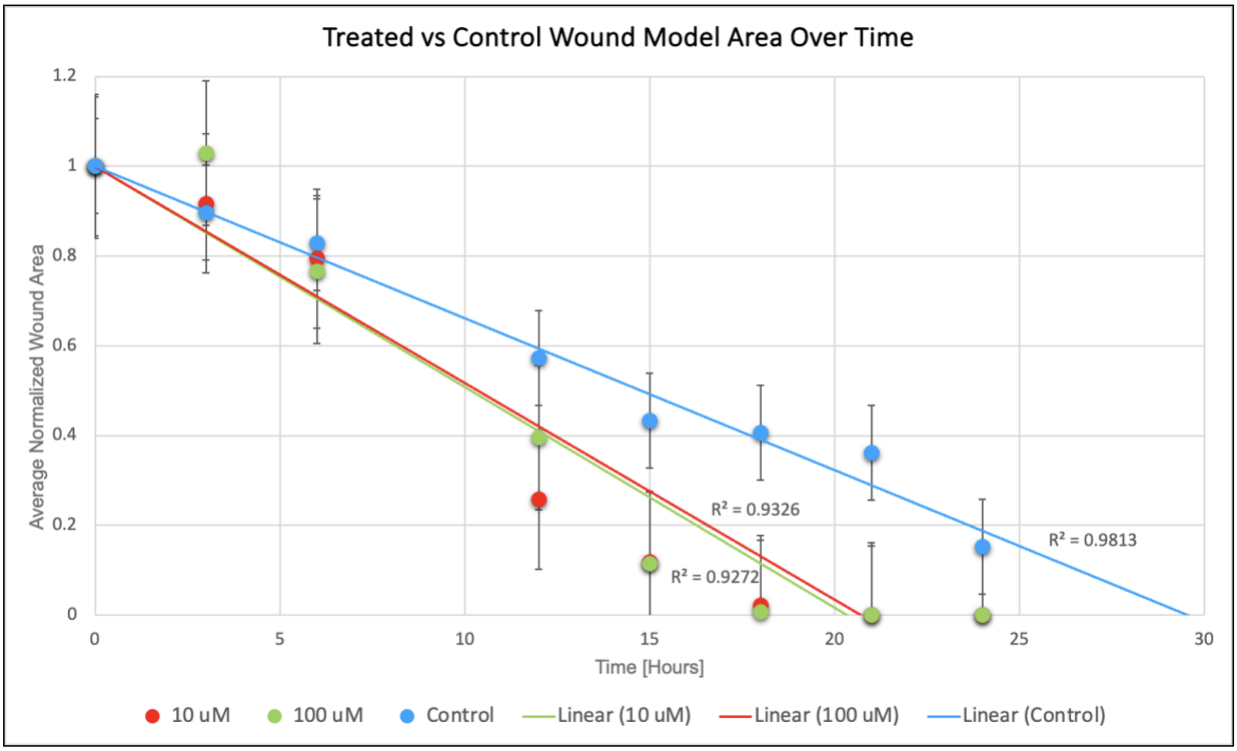


***Figure 8****: Graph of normalized average area over time in hours. Error bars indicate significant differences at time point 15 hours between the treated and control data sets. An unpaired T-Test was performed to determine statistical significance. Each data point represents mean +/- SD at least xx cells from 3 independent experiments. The sample treated with 10 uM or 100 uM showed $p < 0.05$. However, when comparing the two treatment data sets against one another, $p > 0.31$, which supports the claim that the lower dosage of P188 has the same effect as a more concentrated treatment.*

## 4.5 Computer Automated Wound Edge Detection

The computer-automated analysis of wound edges was illustrated by comparing images at Time = 0 and Time = 18 hours. Clear results were observed initially, then following T = 0 considerations were raised about the sustained accuracy of the method over time. This method is

still in developmental stages and this progress is only meant to be used as proof of progress and potential in the future versions of this analysis method.

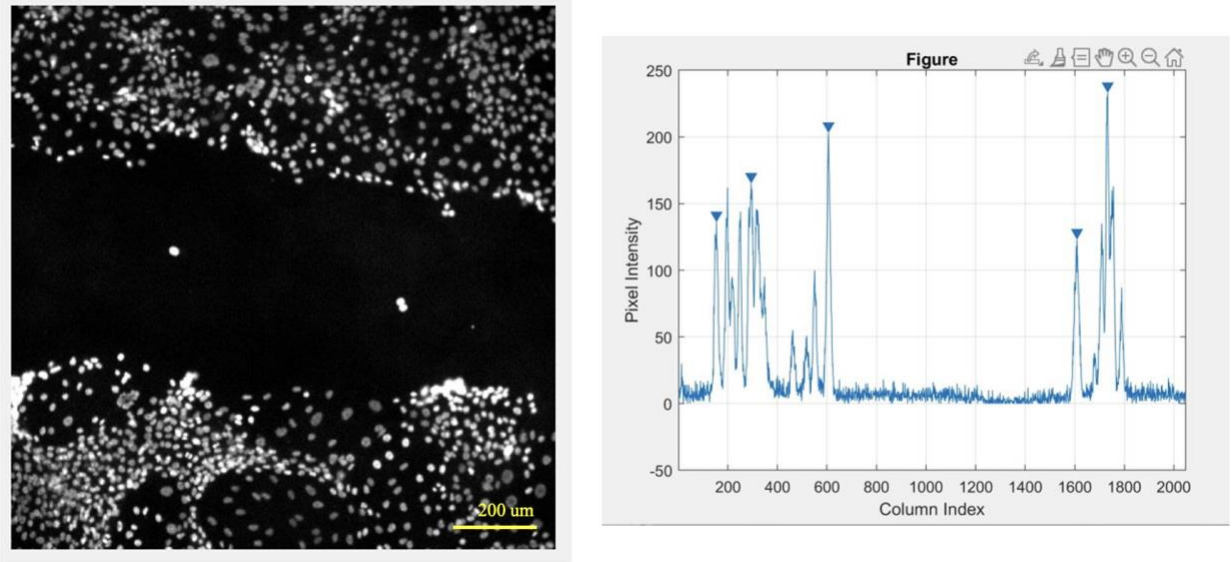


***Figure 9****: Image of wound at Time = 0 with computer automated analysis and resulting graph of average pixel intensity per row. Bar = 200 um.*

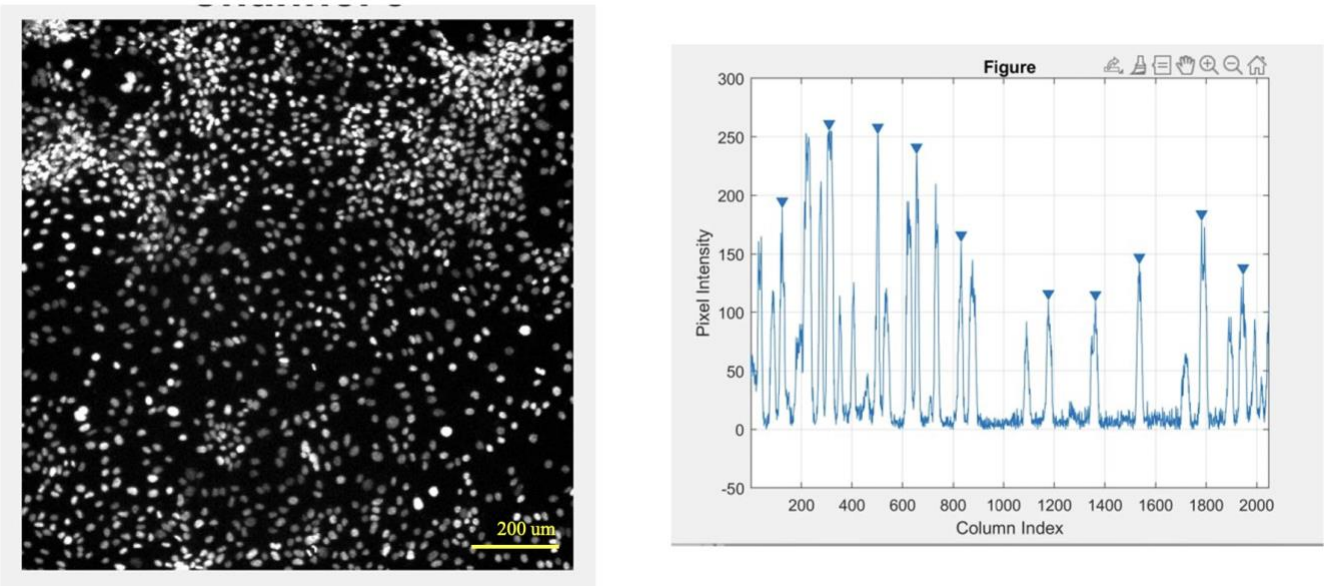


***Figure 10****: Image of wound at Time = 18 hours with computer automated analysis and resulting graph of average pixel intensity per row. Bar = 200 um. It represents an adequate methodology to determine the wound size, especially at later times.*

4.6 FIJI Cell Count Analysis

Cell count analysis, conducted using ImageJ features, provided a visual representation of cell proliferation in the region of interest (ROI) over time, despite acknowledged limitations in accuracy.

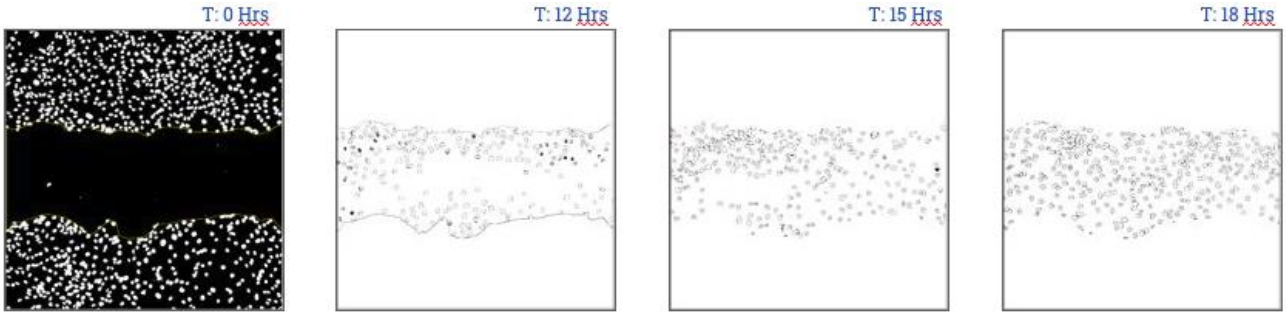


***Figure 11****: Treated 10 uM series of images over time demonstrating ImageJ's cell count increase within T = 0 ROI.*

T-tests were also performed on the data collected from the cell count analysis but because of the inconsistency in data collection, the results only support further need for a more objective form of analysis in the future.

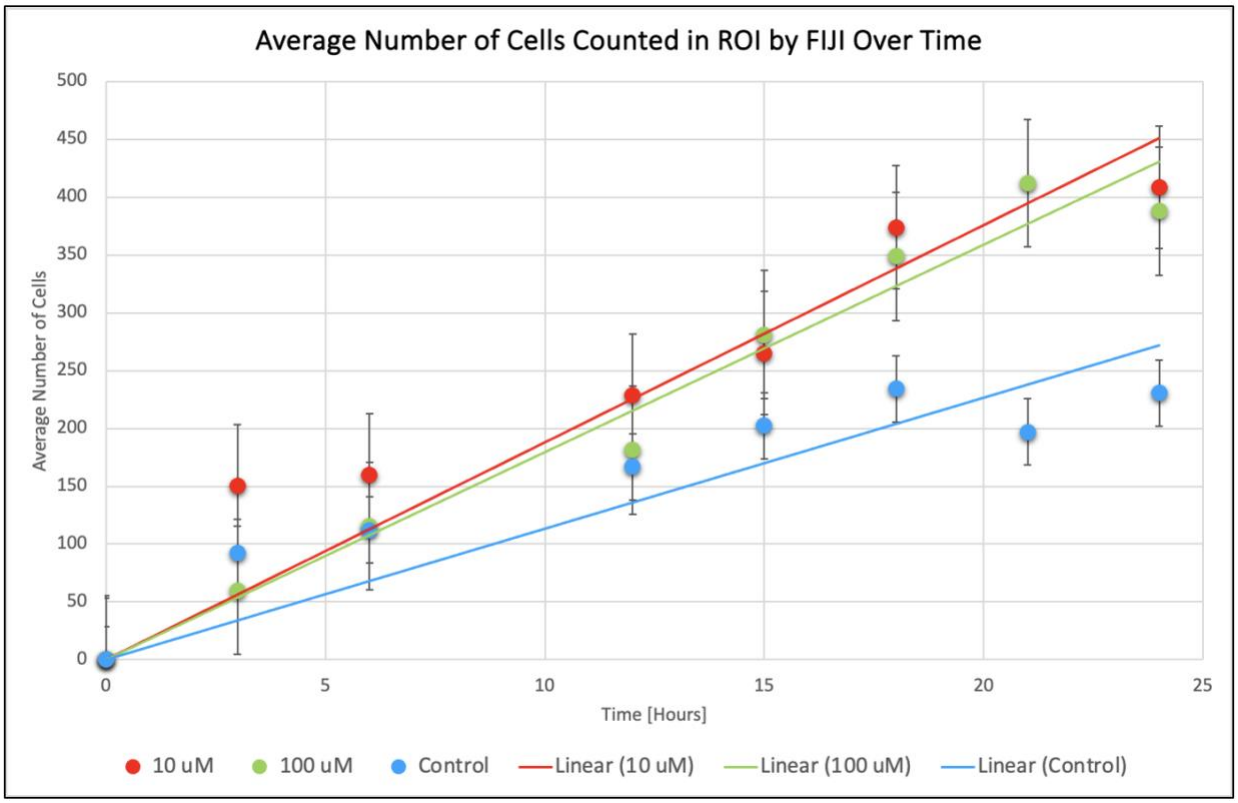


***Figure 12**: Graph of average cell count over time. A linear regression was sufficient to describe repopulation of the wound area with live cells. While no statistical significance was found, there appears to be a trend of increasing number of cells found in the wound area, which may lead to a postulate that the wound closure is mediated by a combination of enhanced cell proliferation and migration.*

# Chapter 5: Conclusion

## 5.1 Discussion

In this study, the impact of Poloxamer 188 (P188) on wound healing dynamics using a scratch model on BALB/C Mouse Brain Endothelial Cells (MBMECs) was investigated. The experimental design involved creating controlled scratch wounds on endothelial cell monolayers and assessing the influence of varying concentrations of P188 on the subsequent healing process. The results consistently demonstrated that P188 treatment significantly influences the rate and efficacy of wound closure in MBMECs as well as revealing no significant dependence on the concentration of dosage between 10 uM and 100 uM. The scratch model provided a robust platform for observing cellular responses to injury and gauging the therapeutic potential of P188 in promoting wound healing. The observed effects of P188 on wound closure align with its known cytoprotective properties reported in various applications. The ability of P188 to modulate inflammation, act as an antithrombotic agent, and improve microvascular blood flow contributes to its multifaceted impact on the wound healing process. The precise mechanisms underlying P188's influence on endothelial cell migration and proliferation warrant further investigation.

The important first step of creating the wound model for the extent of this research was to establish a consistent monolayer through confirmation of visual confluency in a bright field image and in tight junction formation with ZO-1 immunostaining (see Fig. 5). This form of qualitative judgement is common practice, although automated quantitative methods of confirming confluency are being explored [25].

The formation of a consistent monolayer is important because scratch models are difficult to reproduce due to the high degree of variability. Results from previous studies indicate the rate

of re-colonization is very sensitive to the initial cell density [25], so in order to determine an accurate rate of wound closure, the initial density and procedure up to the time of the wounding, is crucial to the resulting data gathered.

Another important variable in determining the rate of closure in the wound model was gathering data from images of the same location at each time point. This proved challenging as time progressed due to the wound being visually confirmed at early time points, but becoming difficult to locate as the wound reached closure. One method explored involved using cell culture slides with gridded lines on the bottom so the wound area was able to be tracked in a coordinate-style system. This method failed as the gridded lines were too coarse. Microfabrication techniques have now become routine and may be applied in future to design a better wound edge tracking methodology [26][27].

The chosen method, that led to the most accurate location of the wound involved making tick marks on the outside of the petri dish that corresponded with the stage of the microscope and then recording which arm of the wound was being tracked. For example, a description of each plate was recorded at Time = 0 that looked like "Right, Mid" which would correspond to the middle section of the right arm of the "+" shaped wound. Inspiration for the methods behind the wound model come from assays performed using HeLa cells studying migration patterns, utilizing the "+" shaped wound pattern [28].

The analysis of images by creating hand-drawn ROI's interpreted by ImageJ FIJI is a commonly used, widely available method but leaves room for human error and biases when the user is drawing said area. The chosen method was further complicated by normalizing the average area of the wound at each time point, to find a percent of the initial wound area. New methods of wound area determination are being explored including the development of programs

capable of image segmentation like the GrowCut algorithm used to characterize cell migration in scratch assays. The process involves specifying initial pixels (seeds) for cell and background regions, evolving through iterations wherein surrounding pixels are assigned to classes based on their intensity similarity to seed pixels [29]. If the scope of the project had allowed for more time to explore such programs as GrowCut and others, it would have provided further in-site into determining the exact rate of growth as a linear or otherwise function.

## 5.2 Future Work

Based on the findings of lower concentrations of P188 treatment leading to the same rate of wound closure as a higher concentration the next logical step would be to determine how much lower the concentration can be taken until ineffective. Because of the time constraint of this project, concentrations lower than 10 uM were not explored but given the time and resources it would be crucial to define. The next step in researching the poloxamer would be to determine the mechanism of wound healing, it has been shown that the poloxamer acts as a membrane plug, allowing the injured cell to sustain the intrinsic cell repair machinery [30].

Exploring alternate methods of mechanism, in literature review of previous wound models, researchers focus on the cell's natural ability to migrate without too much mention of whether or not cell proliferation occurs or how it could even be detected.

These cell migration patterns are typically tracked in much shorter windows of time with expensive resources such as incubatory microscopes that allow for the culture plate or slide to remain under surveillance for as long as needed, without having to be moved. Although this setup would be ideal and it would remove the human error in having to re-position each time before imaging, it is unattainable at this current point in time so alternative methods must be incorporated. It should also be re-enforced that the initial cell density has proven to have effects

on the migration patterns after wounding so it would be critical that further experimentation is done exploring the effects of a higher or lower seeding density with the addition of the poloxamer against a negative control to further optimize the results. Expanding on the effects of seeding density on migration patterns, work in the future should examine the wound width threshold. If the width of the wound that will not close under normal conditions is determined, it can be further investigated whether or not the P188 treatment has an effect on the new conditions.

The idea of the P188 treatment promoting cell proliferation is supported by on-going studies examining the level of activity in the mitochondria using MTT assays [31][32] that fluorescently label cells with higher levels of activity. Preliminary data from Dr. Nagham Alatrash supports the idea of increased activity in proliferation as well.

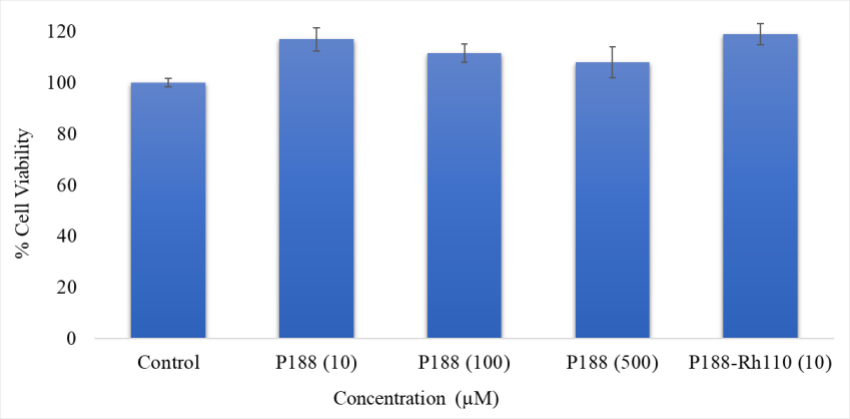


***Figure 13**: Cell viability experiments were performed using mouse brain endothelial cells (MBECs). Cells were treated with 10, 100, and 500 μM P188 for 24 hours, and the viability was determined using MTS assay. In the range of P188 concentrations applied to determine cell viability, no statistical difference was observed, indicating that P188 does not adversely affect the cell viability. However, the results do demonstrate a trend in which cell proliferation was facilitated by the P188 treatment.*

In conclusion, P188 continues to show its potential for wound healing. By establishing a new procedure utilizing BEC's in a systematic method, the effects of P188 are proved significant. Through the completion of further experiments, the mechanism of wound closure will be better defined in endothelial cells which may open doors to extend P188-mediated wound healing to different tissue types in response to mechanical, chemical, or biological stresses or traumas.

# Chapter 6: References


[1] N. J. Abbott, A. A. K. Patabendige, D. E. M. Dolman, S. R. Yusof, and D. J. Begley, "Structure and function of the blood-brain barrier," *Neurobiol. Dis.*, vol. 37, no. 1, pp. 13–25, Jan. 2010, doi: 10.1016/j.nbd.2009.07.030.

[2] P. Ballabh, A. Braun, and M. Nedergaard, "The blood-brain barrier: an overview: structure, regulation, and clinical implications," *Neurobiol. Dis.*, vol. 16, no. 1, pp. 1–13, Jun. 2004, doi: 10.1016/j.nbd.2003.12.016.

[3] B. V. Zlokovic, "The blood-brain barrier in health and chronic neurodegenerative disorders," *Neuron*, vol. 57, no. 2, pp. 178–201, Jan. 2008, doi: 10.1016/j.neuron.2008.01.003.

[4] M. D. Sweeney, A. P. Sagare, and B. V. Zlokovic, "Blood-brain barrier breakdown in Alzheimer disease and other neurodegenerative disorders," *Nat. Rev. Neurol.*, vol. 14, no. 3, pp. 133–150, Mar. 2018, doi: 10.1038/nrneurol.2017.188.

[5] B. Obermeier, R. Daneman, and R. M. Ransohoff, "Development, maintenance and disruption of the blood-brain barrier," *Nat. Med.*, vol. 19, no. 12, pp. 1584–1596, Dec. 2013, doi: 10.1038/nm.3407.

[6] R. Daneman and A. Prat, "The Blood–Brain Barrier," *Cold Spring Harb. Perspect. Biol.*, vol. 7, no. 1, p. a020412, Jan. 2015, doi: 10.1101/cshperspect.a020412.

[7] B. Engelhardt and L. Sorokin, "The blood-brain and the blood-cerebrospinal fluid barriers: function and dysfunction," *Semin. Immunopathol.*, vol. 31, no. 4, pp. 497–511, Nov. 2009, doi: 10.1007/s00281-009-0177-0.

[8] O. Tornavaca *et al.*, "ZO-1 controls endothelial adherens junctions, cell–cell tension, angiogenesis, and barrier formation," *J. Cell Biol.*, vol. 208, no. 6, pp. 821–838, Mar. 2015, doi: 10.1083/jcb.201404140.

[9] A. Alahmari, "Blood-Brain Barrier Overview: Structural and Functional Correlation," *Neural Plast.*, vol. 2021, pp. 1–10, Dec. 2021, doi: 10.1155/2021/6564585.

[10] A. Tremel *et al.*, "Cell migration and proliferation during monolayer formation and wound healing," *Chem. Eng. Sci.*, vol. 64, no. 2, pp. 247–253, Jan. 2009, doi: 10.1016/j.ces.2008.10.008.

[11] M. Oberringer, C. Meins, M. Bubel, and T. Pohlemann, "A new in vitro wound model based on the co-culture of human dermal microvascular endothelial cells and human dermal fibroblasts," *Biol. Cell*, vol. 99, no. 4, pp. 197–207, 2007, doi: 10.1042/BC20060116.

[12] C.-C. Liang, A. Y. Park, and J.-L. Guan, "In vitro scratch assay: a convenient and inexpensive method for analysis of cell migration in vitro," *Nat. Protoc.*, vol. 2, no. 2, Art. no. 2, Feb. 2007, doi: 10.1038/nprot.2007.30.

[13] W. J. Ashby and A. Zijlstra, "Established and Novel Methods of Interrogating Two-Dimensional Cell Migration," *Integr. Biol. Quant. Biosci. Nano Macro*, vol. 4, no. 11, pp. 1338–1350, Nov. 2012, doi: 10.1039/c2ib20154b.

[14] B. L. Coomber and A. I. Gotlieb, "In vitro endothelial wound repair. Interaction of cell migration and proliferation.," *Arterioscler. Off. J. Am. Heart Assoc. Inc*, vol. 10, no. 2, pp. 215–222, Mar. 1990, doi: 10.1161/01.ATV.10.2.215.

[15] M. L. C. Albuquerque, C. M. Waters, U. Savla, H. W. Schnaper, and A. S. Flozak, "Shear stress enhances human endothelial cell wound closure in vitro," *Am. J. Physiol.-Heart Circ. Physiol.*, vol. 279, no. 1, pp. H293–H302, Jul. 2000, doi: 10.1152/ajpheart.2000.279.1.H293.

[16] P. Martin, “Wound healing--aiming for perfect skin regeneration,” *Science*, vol. 276, no. 5309, pp. 75–81, Apr. 1997, doi: 10.1126/science.276.5309.75.
[17] R. Zhang, R. L. Hunter, E. A. Gonzalez, and F. A. Moore, “Poloxamer 188 prolongs survival of hypotensive resuscitation and decreases vital tissue injury after full resuscitation,” *Shock Augusta Ga*, vol. 32, no. 4, pp. 442–450, Oct. 2009, doi: 10.1097/SHK.0b013e31819e13b1.
[18] G. Serbest, J. Horwitz, M. Jost, and K. A. Barbee, “Mechanisms of cell death and neuroprotection by poloxamer 188 after mechanical trauma,” *FASEB J.*, vol. 20, no. 2, pp. 308–310, 2006, doi: 10.1096/fj.05-4024fje.
[19] H.-J. Bao *et al.*, “Poloxamer-188 Attenuates TBI-Induced Blood–Brain Barrier Damage Leading to Decreased Brain Edema and Reduced Cellular Death,” *Neurochem. Res.*, vol. 37, no. 12, pp. 2856–2867, Dec. 2012, doi: 10.1007/s11064-012-0880-4.
[20] R. L. Hunter, A. Z. Luo, R. Zhang, R. A. Kozar, and F. A. Moore, “Poloxamer 188 Inhibition of Ischemia/Reperfusion Injury: Evidence for a Novel Anti-adhesive Mechanism,” *Ann. Clin. Lab. Sci.*, vol. 40, no. 2, pp. 115–125, Mar. 2010.
[21] C. Luo *et al.*, “Poloxamer 188 Attenuates Cerebral Hypoxia/Ischemia Injury in Parallel with Preventing Mitochondrial Membrane Permeabilization and Autophagic Activation,” *J. Mol. Neurosci.*, vol. 56, no. 4, pp. 988–998, Aug. 2015, doi: 10.1007/s12031-015-0568-8.
[22] “Scientific Image and Illustration Software | BioRender.” Accessed: Nov. 10, 2023. [Online]. Available: https://www.biorender.com/
[23] E. Inyang, V. Abhyankar, B. Chen, and M. Cho, “Modulation of in vitro Brain Endothelium by Mechanical Trauma: Structural and Functional Restoration by Poloxamer 188,” *Sci. Rep.*, vol. 10, no. 1, Art. no. 1, Feb. 2020, doi: 10.1038/s41598-020-59888-2.
[24] J. Krithikadatta, “Normal Distribution,” *J. Conserv. Dent. JCD*, vol. 17, no. 1, pp. 96–97, 2014, doi: 10.4103/0972-0707.124171.
[25] W. Jin, E. T. Shah, C. J. Penington, S. W. McCue, L. K. Chopin, and M. J. Simpson, “Reproducibility of scratch assays is affected by the initial degree of confluence: Experiments, modelling and model selection,” *J. Theor. Biol.*, vol. 390, pp. 136–145, Feb. 2016, doi: 10.1016/j.jtbi.2015.10.040.
[26] M. Bao, J. Xie, A. Piruska, X. Hu, and W. T. S. Huck, “Microfabricated Gaps Reveal the Effect of Geometrical Control in Wound Healing,” *Adv. Healthc. Mater.*, vol. 10, no. 4, p. 2000630, 2021, doi: 10.1002/adhm.202000630.
[27] S. R. K. Vedula *et al.*, “Emerging modes of collective cell migration induced by geometrical constraints,” *Proc. Natl. Acad. Sci.*, vol. 109, no. 32, pp. 12974–12979, Aug. 2012, doi: 10.1073/pnas.1119313109.
[28] Y. K. Suh *et al.*, “Introducing Wound Healing Assays in the Undergraduate Biology Laboratory Using Ibidi Plates,” *J. Microbiol. Biol. Educ.*, vol. 23, no. 2, pp. e00061-22, Aug. 2022, doi: 10.1128/jmbe.00061-22.
[29] A. V. P. Bobadilla *et al.*, “In vitro cell migration quantification method for scratch assays,” *J. R. Soc. Interface*, vol. 16, no. 151, p. 20180709, Feb. 2019, doi: 10.1098/rsif.2018.0709.
[30] J. G. Moloughney and N. Weisleder, “Poloxamer 188 (P188) as a Membrane Resealing Reagent in Biomedical Applications,” *Recent Pat. Biotechnol.*, vol. 6, no. 3, pp. 200–211, Dec. 2012, doi: 10.2174/187220812803900892.
[31] T. L. Riss *et al.*, “Cell Viability Assays,” in *Assay Guidance Manual [Internet]*, Eli Lilly & Company and the National Center for Advancing Translational Sciences, 2016. Accessed: Nov. 27, 2023. [Online]. Available: https://www.ncbi.nlm.nih.gov/books/NBK144065/

[32] “Cell Viability Assays - Assay Guidance Manual - NCBI Bookshelf - MTT Assay Protocol for Cell Viability and Proliferation.” Accessed: Nov. 27, 2023. [Online]. Available: https://afifilm.org/mtt-cytotoxicity-assay-protocol